Chapter IV

Copper(II) Complexes with a Benzimidazole Functionalized Schiff base: Synthesis, Crystal Structures, and Role of Ancillary ions in Phenoxazinone Synthase Activity

4.1. Introduction

In this modern age of science, copper(II) based coordination compounds represents a promising class of smart molecules with significant contributions in designing functional materials like catalytic, magnetic, optic, conducting materials and so on.[1–5] In the biological world, copper(II) ion remains one of the most prevalent metal ions and its compounds play significant roles in different metal-dependent proteins such as the active site in hemocyanin[6] as an oxygen carrier, perform aromatic ring oxidations in tyrosinase,[7] catechol oxidase,[8] oxygenase enzyme in quercetin 2,3-dioxygenase,[9-11], hydrogen peroxide producer in galactose and glyoxal oxidases[12-15] and methane oxidation as methane monooxygenase, pMMO.[16-18] Among the different copper-based metalloproteins and metalloenzymes in the living system, phenoxazinone synthase acts as an important metalloenzyme.[19] Phenoxazinone synthase catalyzes the oxidation of 2-aminophenols to 2-aminophenoxazinone species Actinomycin D, a naturally occurring antineoplastic agent, which inhibits DNA directed RNA synthesis and is also used clinically for the treatment of certain types of cancer.[20-25]

On the other hand, benzimidazole and its derivatives are considered as a significant class of N-containing heterocyclic compounds because of their broad range of biological activities such as antimicrobial,[26] antivirus,[27] antifungals,[28] anti-inflammatory,[29] anticancer,[29] antiulcer,[30] proton pump inhibitors[31] and anticoagulants activities.[32] They are also the key intermediate in many organic reactions and are used for the industrial synthesis of numerous products.[33] Therefore, various scientific groups are engrossed in the synthesis and metallation of benzimidazoles with novel functionality to develop smart molecules with improved biomimetic and pharmacological activities that remain an urgent priority. Until to date, several methods are employed to synthesis different substituted benzimidazoles using either a catalyst or high temperature which made the process economically and

environmentally less attractive.[34-37] Since, copper(II) and benzimidazole play a significant role in many disciplines, it is important to study the copper–benzimidazole interaction and chemists have made use of this interaction to build up some fascinating classes of molecules which show many interesting properties.[38-40] As a part of our interest in developed copper-based coordination compounds for mimicking the bio-inspired oxidation reactions, we reported a straightforward synthesis of 1-(4-methoxybenzyl)-2-(4-methoxyphenyl)benzimidazole ($\mathbf{L^3}$) ligand under ambient conditions. To elucidate the use of such type of ligand in coordination and applied chemistry research field, I have prepared two structurally similar mononuclear copper(II) complexes with $\mathbf{L^3}$, namely $[Cu(\mathbf{L^3})_2Cl_2]_2$ (**2**) and $[Cu(\mathbf{L^3})_2(NO_3)_2]_2$ (**3**) and structurally characterized by X-ray diffraction technique with other spectroscopic methods. Attempts have also been made to illustrate the presence of ancillary ligands in the primary zone of coordination of Cu(II) centre for the oxidative catalysis of 2-aminophenol in methanol medium. Both the complexes were found to show impressive phenoxazinone synthase mimicking activity towards oxidative coupling of 2-aminophenol. [$\mathbf{L^3}$= 1-(4-methoxybenzyl)-2-(4-methoxyphenyl)-1H-benzo[d]imidazole, **Scheme 4.1**]

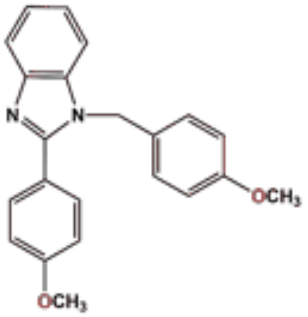

Scheme 4.1. Schematic diagram of the ligand $\mathbf{L^3}$

4.2. Experimental Section

4.2.1. Preparation of the complex

4.2.1.1. Materials and Methods

Highly pure *o*-phenylenediamine (Sigma Aldrich, USA), *p*-anisaldehyde (Sigma Aldrich, USA), copper(II) chloride dihydrate (Merck, India), copper(II) nitratre trihydrate (Merck, India) and *o*-aminophenol (Sigma Aldrich, USA) were purchased from the respective outlets. All the chemicals and solvents used in this study were of analytical grade.

4.2.1.2. Synthesis of the ligand L^3, copper complexes 2 and 3

The ligand, $\mathbf{L^3}$ was prepared following the reported procedure with slight modification.[41-43] The Schiff base was prepared by refluxing *o*-phenylenediamine (0.108g, 1mmol) with *p*-anisaldehyde (0.272 g, 2mmol) in 25 ml ethanol for 6h. The brown-coloured compound was extracted from the solution and stored in vaccuo over $CaCl_2$. The copper complexes were synthesized in methanolic solution of $CuCl_2.2H_2O$ (0.170 g, 1mmol) / $Cu(NO_3)_2.3H_2O$ (0.241g, 1mmol) was mixed dropwise to dichloromethane solution of $\mathbf{L^3}$ (0.688g, 2 mmol). The yellow-coloured solution of the Schiff base immediately turned green for both the reactions and the resulting solutions were further stirred for 45 minutes followed by filtering. The filtrate was kept for slow evaporation in an open atmosphere. After 5-7 days, microcrystalline green coloured crystals for **2** and **3** were separated which were dried over silica gel.

Yield of $\mathbf{L^3}$: 0.219 g (~85.2%).

Yield of **2**: 0.1310 g (~77.0% metal salt based)

Yield of **3**: 0.1850 g (~76.80% metal salt based)

4.2.2. Physical measurements

FT-IR spectra of the $\mathbf{L^3}$**, 2 and 3** were recorded using FTIR-8400S SHIMADZU spectrometer in the range of 400-3600 cm^{-1}. ^1H and ^{13}C NMR spectrum of ligand were obtained on a Bruker Advance 400 MHz spectrometer in $CDCl_3$ at 298 K. Steady-state absorption and other spectral data were recorded with a JASCO V-730 spectrophotometer. ESI-MS spectral measurements were performed with a Q-TOF-micro quadruple mass spectrometer. A Perkin Elmer 2400 CHN microanalyser was employed to carry out the elemental analyses of the compounds. The pH values of different solutions were measured by Labman pH meter at room temperature. X-band EPR spectral measurements for the copper complexes were done with a Magnettech GmbH MiniScope MS400 spectrometer where the microwave frequency was measured with an FC400 frequency counter.

Table 4.1. CHN analysis of $\mathbf{L^3}$, complexes **2** and **3**

Compound (Mol formula)	Found (Calcd)%		
	C	H	N
$\mathbf{L^3}$ ($C_{22}H_{20}N_2O_2$)	76.70 (76.72)	5.80 (5.85)	8.11 (8.13)

Complex 2 ($C_{44}H_{40}N_4O_4CuCl_2$)	64.45 (64.47)	5.16 (2.17)	6.63 (6.68)
Complex 3 ($C_{44}H_{40}N_6O_{10}Cu$)	60.28 (60.30)	4.59 (4.60)	9.55 (9.59)

4.2.3. X-ray structural studies and refinement

A Rigaku XtaLABmini diffractometer equipped with Mercury 375R (2×2 bin mode) CCD detector was employed to collect X-ray diffraction data for the copper(II) complexes with graphite monochromated Mo-Kα radiation (λ=0.71073 Å) at 100 K for **2** and at 150 K for **3** using ω scans. The data were reduced using CrysAlisPro 1.171.39.35c and 1.171.39.7f[44] and the space groups were determined using Olex2. The crystal structures were resolved by dual space method using SHELXT-2015.[45] The crystallographic data were refined by full-matrix least-squares procedures using the SHELXL-2015[46] software package through OLEX2 suite.[47]

4.2.4. Hirshfeld surface analysis of the complexes 2 and 3

Hirshfeld surfaces[48] and 2D fingerprint plots[49] for the copper complexes **2** & **3** have been generated by Crystal Explorer 17.5[50] program package employing their X-ray diffraction data. The location of intermolecular interactions within crystal packing was examined through Hirshfeld Surface analysis. The details of Hirshfield surface analysis were described elsewhere.[48-50]

4.2.5. Catalytic oxidation studies of 2-aminophenol

The catalytic oxidation of 2-aminophenol was performed by treatment of 1×10^{-4} M solution of copper(II) complexes with 1×10^{-3} M of 2-aminophenol (2-AP) solution in methanol (MeOH). The wavelength scans for the course of catalysis was monitored with a spectrophotometer for 2h from the 300 to 700 nm wavelength range.[50,51]

Kinetic experiments were also carried out spectrophotometrically to comprehend the catalytic efficacy and nature of oxidation of aminophenol by the copper(II) complexes in MeOH at 298 K.[52] 0.04 mL of 1×10^{-4} M constant concentration of copper(II) complexes the solutions were mixed with 2 mL of 10 fold concentrated solution of 2-AP to attain the final concentration as 1×10^{-4} M. The catalytic conversion of 2-aminophenol to its oxidation product was examined with the variation of time at 433 nm for **2** and 430 nm for **3** (time scan) in MeOH.[53,54] The rate of catalytic oxidation based

on substrate concentration was determined by following the initial rate law in triplicate. The kinetics of the catalytic oxidation reactions were carried out at different temperature to determine the activation parameters.

The product, 2-amino-3*H*-phenoxazine-3-one (APX) developed by catalytic oxidation of 2-AP has been extracted with column chromatographic method for both the copper(II) complexes. Neutral alumina as column support and benzene-ethyl acetate an eluant mixture was employed in the chromatographic separation. Proton NMR spectroscopy was evidenced to check the purity of aminophenoxazinone compound (APX). ^{1}H NMR data for APX, ($CDCl_3$, 400 MHz,) ^{1}H: 7.61 (m, 1H), 7.45 (m, 3H), 6.46 (s, 1H), 6.37 (s, 1H), 6.25 (s, 1H).

4.2.6. Detection of hydrogen peroxide in the course of catalysis

The participation of atmospheric oxygen in the oxidative coupling of 2-AP was verified from the detection of hydrogen peroxide with reported literature.[55,56] In the course of oxidation of 2-AP in MeOH, H_2SO_4 was added to attain pH 2. After a certain time, an equal volume of water was mixed to stop further oxidation. The oxidation product, phenoxazinone compound was extracted three times with DCM. 10% solution of KI (1 mL) and 3 drops of a 3% solution of ammonium molybdate were mixed with the aqueous layer. The development of I_3^- species at λ_{max}= 353 nm was monitored through a spectrophotometer which may be assignable to the production of hydrogen peroxide.

4.2.7. Electrochemical analysis

The BASi Epsilon-EC instrument containing 0.2M tetrabutylammonium hexafluorophosphate as supporting electrolyte was employed for carrying out electrochemical experiments in the DCM medium. The BASi platinum working electrode, platinum auxiliary electrode, Ag/AgCl reference electrode were used for all the measurements.

4.3. Results and discussion

4.3.1. Synthesis and formulation of the ligand L^3, complexex 2 and 3

The benzimidazole functionalized ligand, $\mathbf{L^3}$ was synthesized by refluxing *o*-phenylenediamine with *p*-anisaldehyde in ethanol. The copper(II) complexes were obtained by adding hydrated copper(II) chloride and nitrate salts to the ligand, $\mathbf{L^3}$ in 1:2

mole ratio in MeOH-DCM under slow stirring conditions (**Scheme 4.2**). The different stoichiometric ratios between hydrated copper(II) salts and $\mathbf{L^3}$ were applied to divulge the mode of coordination of the benzimidazole functionalized ligand with Cu(II) ion. Other copper(II) salts like perchlorate, bromide, acetate and sulphate were also reacted with $\mathbf{L^3}$ to develop the copper(II) complexes of varied dimensions and nuclearities but didn't able to do so. Complexes **2** and **3** displayed good solubility in polar solvents like methanol, acetonitrile, dichloromethane, etc. The compounds may be successfully synthesized in methanol-dichloromethane or methanol-acetonitrile medium.

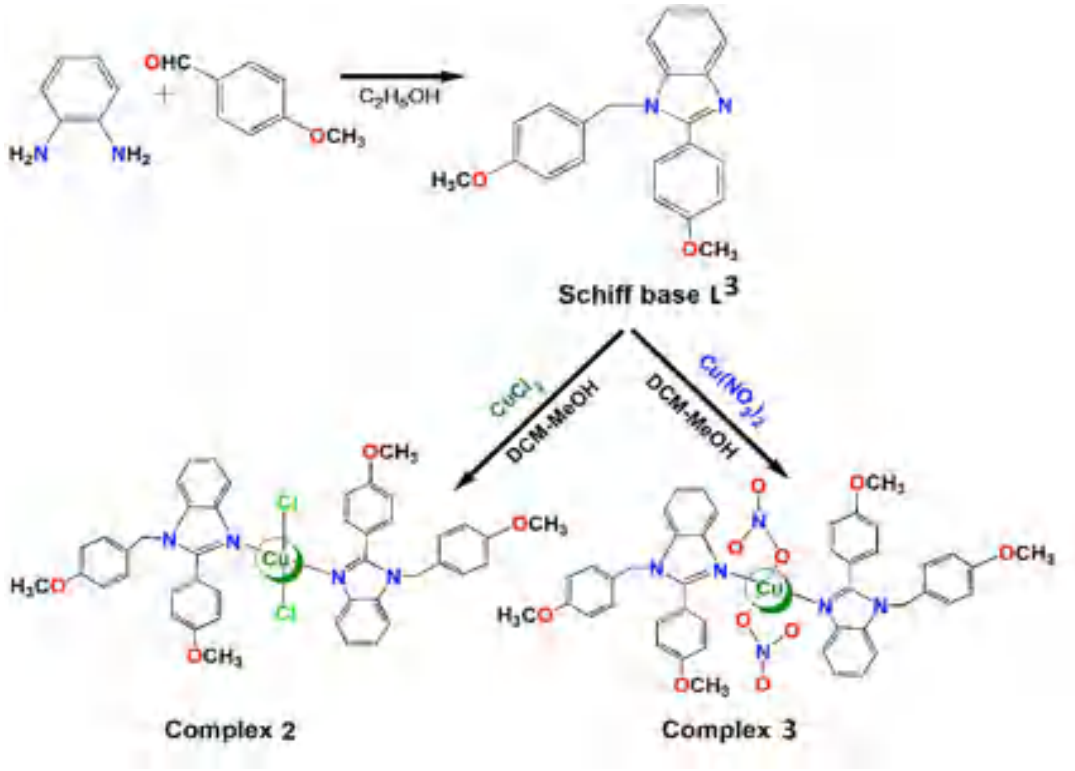

Scheme 4.2. Synthetic route for the complexes **2** and **3**

4.3.2. Infrared spectral analysis of L^3, 2 and 3

Important characteristic peaks of the ligand $\mathbf{L^3}$ ligand were observed at 3058 and 1612 cm^{-1} for methylene and imine groups, respectively. The peak at 3433 cm^{-1} indicates the absorption of moisture by the KBr pellette. The copper complexes **2** & **3** showed strong and sharp characteristic peaks at 3021, 2939 and 3019, 2938 for methylene group. The imine group stretching frequencies were revealed at 1620 and 1617 cm^{-1} in **2** & **3.** These values are displayed in **Table 4.2**.

Table 4.2. Infrared spectral data[a] of L^3 ligand and complexes **2** & **3**

Compounds	ν (cm^{-1})
L^3	3433 –OH, 3058 –CH_2, 1612 –C=N–
Complex 2	3021, 2939 –CH_2, 1620 –C=N–
Complex 3	3019, 2938 –CH_2, 1617 –C=N–

[a]KBr disc

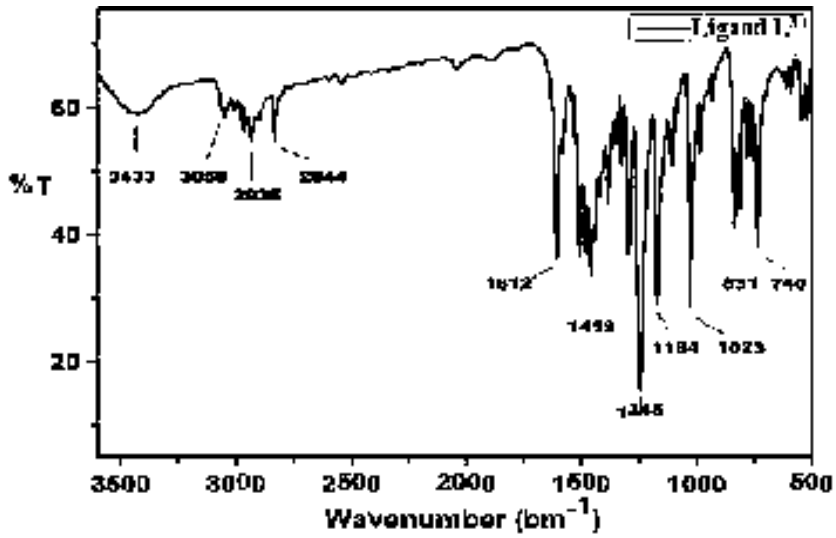

Fig. 4.1. FT-IR spectrum of the ligand, L^3

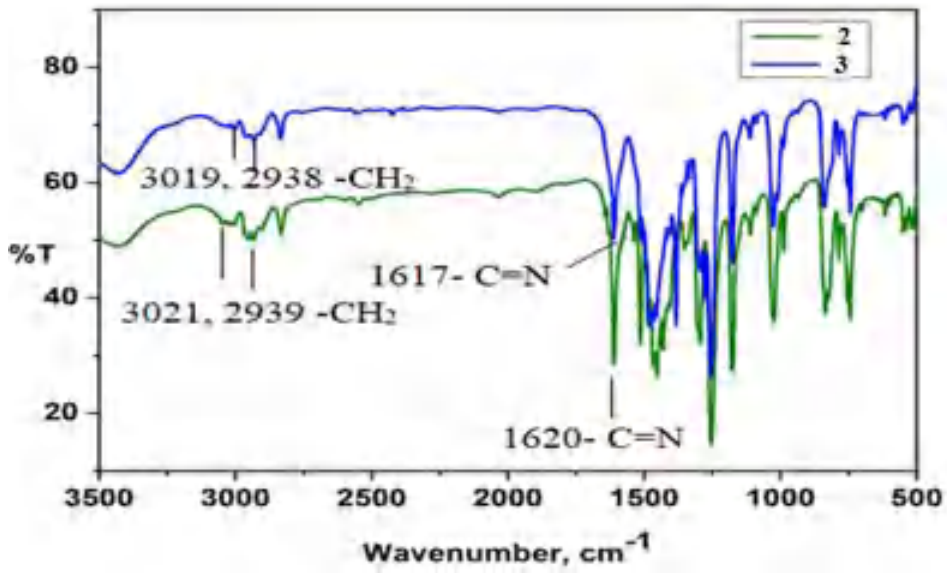

Fig. 4.2. FT-IR spectrum of the complexes **2** & **3**

4.3.3. Electronic spectral analysis

The electronic spectra of the Schiff base L^3 and complexes, **2** & **3** were recorded in acetonitrile medium (MeCN) from 200 to 900 nm at room temperature. The

characteristic bands of $\mathbf{L^3}$ were observed at 258, 289, and 335 nm. The high intensity bands at 258, 289, and 335 were assignable to n-π* and π-π* electronic transitions of ligand origin. The Cu complexes **2** and **3** were showed the characteristic peaks at 286, 605 and 282, 611 nm, respectively. The high intensity bands at 286 for complex **2** and 282 for complex **3** were corresponded to π→π* / n→π* electronic transitions of $\mathbf{L^3}$ ligand while the optical bands at 605 and 611 nm attributed d-d electronic transitions for complex **2** and **3**.

Table 4.3. UV-Vis spectral data[b] of $\mathbf{L^3}$ and **2, 3**

Compounds	λ_{max}, **nm**
$\mathbf{L^3}$	258(1.51), 289(1.26), 335(0.47).
Complex 2	286(1.41), 605(0.02).
Complex 3	282(1.52), 611(0.023).

[b]acetonitrile solution at 298K

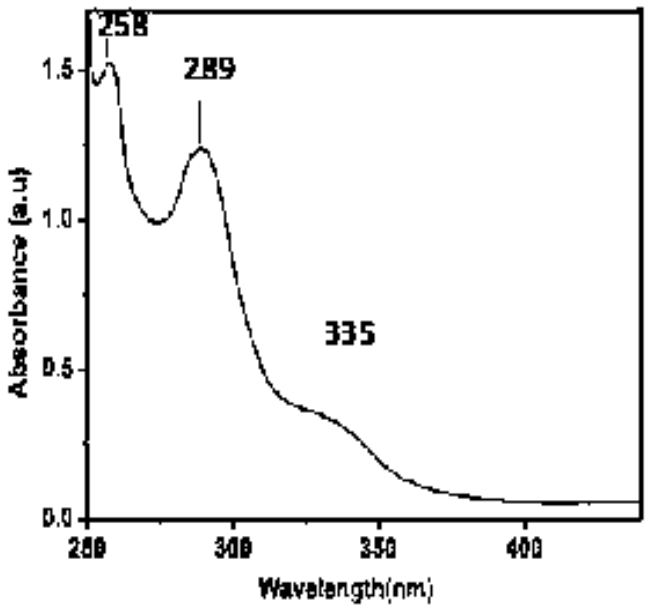

Fig. 4.3. UV-Vis spectrum of the ligand, $\mathbf{L^3}$

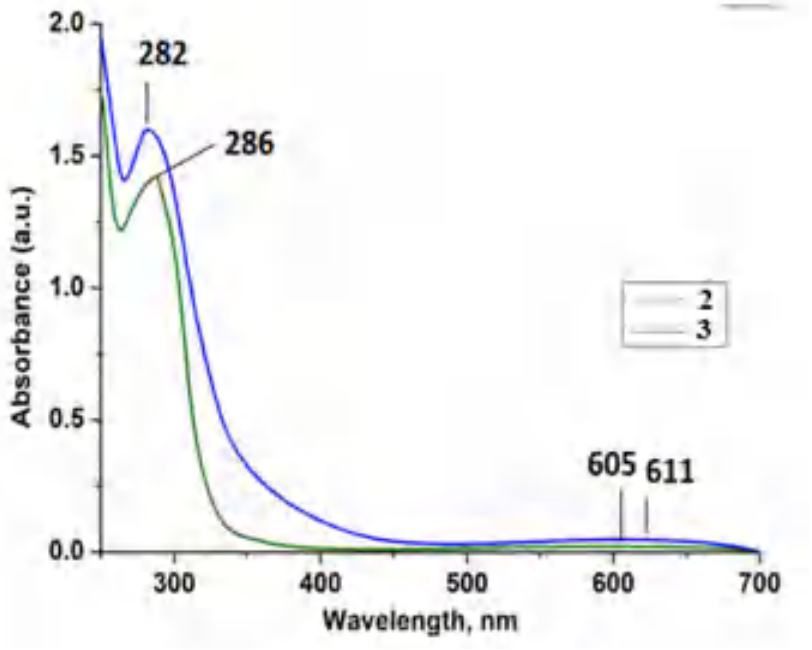

Fig. 4.4. UV-Vis spectra of the complexes, **2** & **3**

4.3.4. NMR spectral analysis

The NMR spectral analysis of $\mathbf{L^3}$ was carried out in $CDCl_3$. **Fig. 4.5** and **4.6** displayed the ^1H and ^{13}C NMR spectra of $\mathbf{L^3}$, respectively. The $\mathbf{L^3}$ displayed a characteristic peak at 5.386 ppm assigning the methylene proton. The proton signals corresponding to aromatic-H appeared in the range 7.84 to 6.84 ppm while the -OCH_3 protons were evident at 3.852 to 3.786 ppm.

The ^{13}C NMR was also recorded to assign the characteristics of the C-atom in $\mathbf{L^3}$. The signals exhibited at 160.887 and 159.113 ppm ph-C bound to -OMe. The azomethine-C and methylene-C were attributed at 154.129 ppm and 56.49 ppm, respectively while the signals in the range 143.212 to 110.394 ppm corresponded to the aromatic-Cs in the $\mathbf{L^3}$.

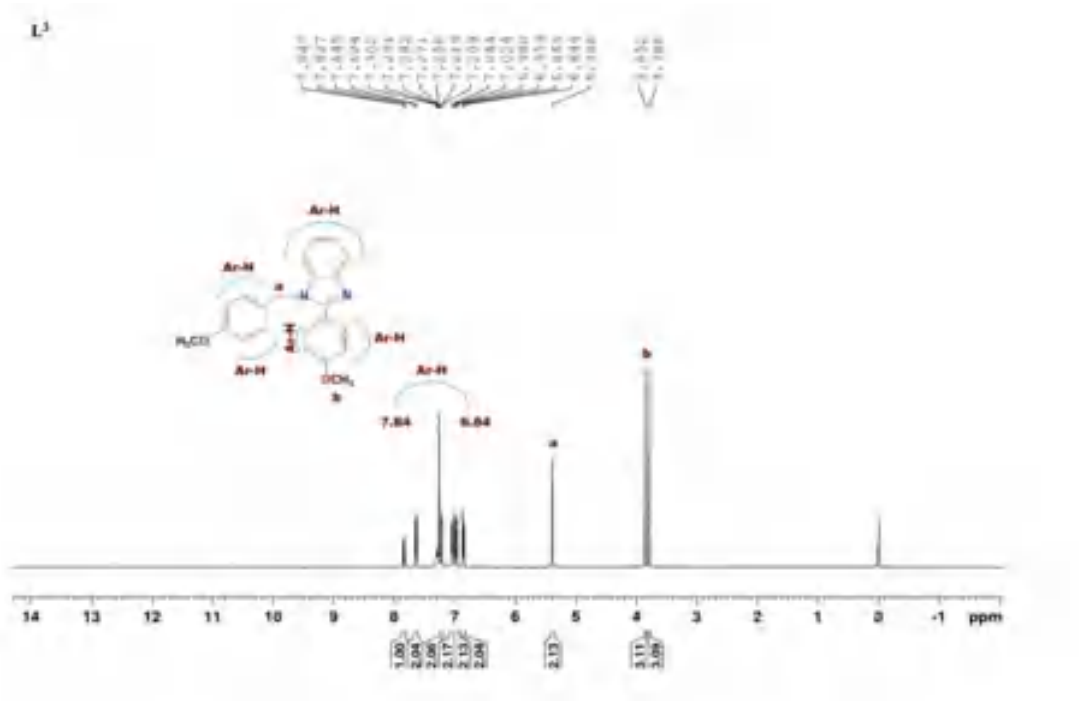

Fig. 4.5. ^{1}H NMR spectrum of the ligand, **L^{3}** in $CDCl_3$

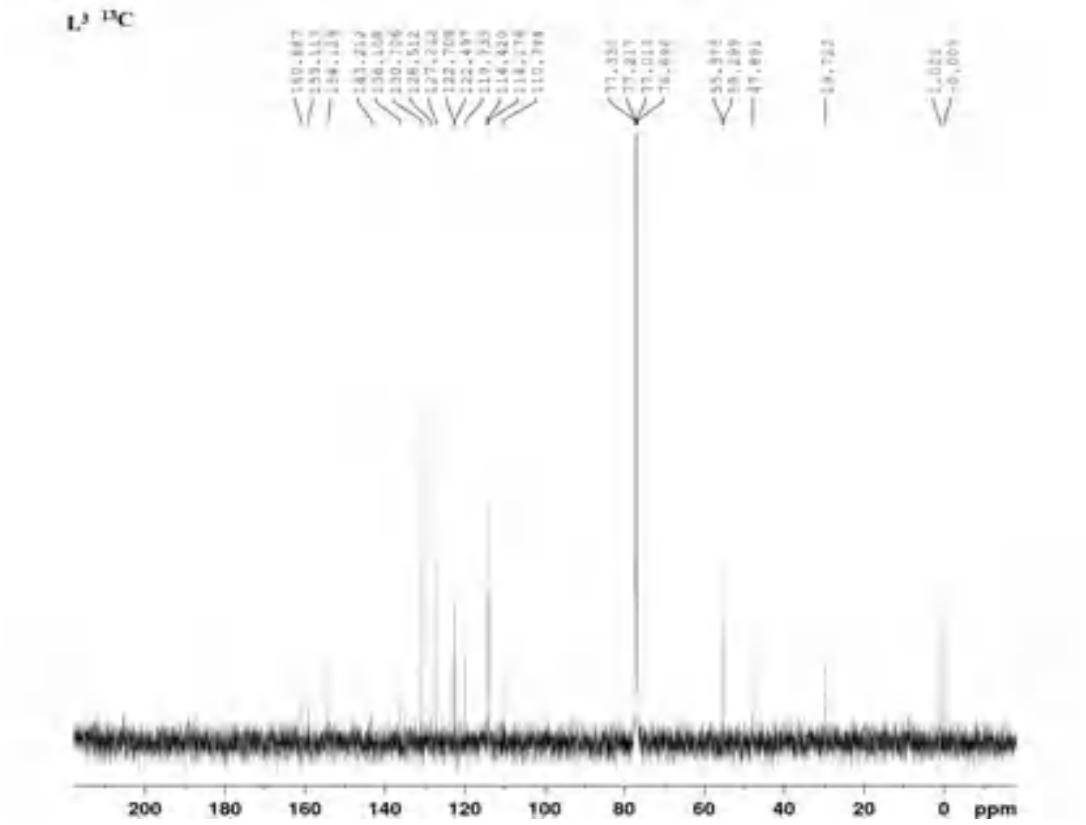

Fig. 4.6. ^{13}C NMR spectrum of the ligand, **L^{3}** in $CDCl_3$

4.3.5. Description of crystal structures

X-ray structural analysis was indicated that both complexes **2** and **3** crystallized in the triclinic system with *P*-1 space group. Crystallographic refinement details were shown in **Table 4.4**. Selected bond lengths and bond angles for complexes **2** and **3** were tabulated in **Table 4.5** and **4.6** respectively. The ORTEP representations of complexes **2** and **3** were shown in **Fig. 4.7** and **8** respectively. Crystal structure studied portray that both copper(II) complexes consist of two asymmetric units of different conformations in **2** and **3**. The copper(II) ion in **2**, was coordinated by two imidazole *N*-atoms of two units of $\mathbf{L^3}$ and two chloride (Cl^-) ions (**Fig. 4.7**), whereas in **3**, the copper centre was coordinated with two imidazole *N*-atoms of two $\mathbf{L^3}$ units and two O-atoms from nitrate (NO_3^-) anions (**Fig. 4.8**). The benzimidazole ligand, $\mathbf{L^3}$ behaves as a terminal monodentate coordinator towards copper(II) ion.

Table 4.4. Crystallographic data and structure refinement parameters for the copper complexes

Parameters	**2**	**3**
CCDC no.	2046275	2046276
Empirical formula	$C_{44}H_{40}N_4O_4Cl_2Cu$	$C_{44}H_{40}N_6O_{10}Cu$
Formula weight	823.24	876.36
T (K)	100.0	150.0
Wavelength (Å)	0.71073	0.71073
Crystal system	Triclinic	Triclinic
Space group	*P*-1	*P*-1
Unit cell dimensions		
a (Å))	9.1963(3)	9.0794(4)
b (Å)	10.0533(6)	10.2760(5)
c (Å)	21.9806(7)	22.4587(11)
α (°)	100.666(4)	79.878(4)
β (°)	90.164(3)	89.780(4)
γ (°)	102.356(4)	77.426(4)
V ($Å^3$)	1948.90(15)	2012.02(17)
Z	2	2

ρ (gm cm^{-3})	1.403	1.447
Absorption coefficient (mm^{-1})	0.747	0.612
F(000)	854	910
Crystal size (mm^3)	0.1×0.2×0.21	0.18×0.27×0.32
Theta range for data collection	2.5 to 32.8°.	3.1 to 27.6°.
Goodness-of-fit on F^2	1.057	1.074
Reflections collected	34507	25004
Independent reflections	12780	9226
Final R indexes [I>=2σ (I)]	R_1 = 0.0650, wR_2 =0.1491	R_1 = 0.0592, wR_2 =0.1767
Largest diff. peak/hole / e $Å^{-3}$	0.90/-0.70	2.53/-0.50

Weighting Scheme: R= Σ|Fo|-|Fc||/Σ|Fo, wR2=$[\Sigma w(Fo^2-Fc^2)^2/\Sigma w(Fo^2)^2]^{1/2}$, Calc. w = $1/[\sigma^2(Fo^2) + (0.0545P)^2 + 0.8856P]$ (**2**); where P = $(Fo^2+2Fc^2)/3$. Calc. w = $1/[\sigma^2(Fo^2) + (0.0887P)^2 + 1.0996P]$ (**3**); where P = $(Fo^2+2Fc^2)/3$.

Table 4.5. Bond distances and bond angles for the complex **2**

Bond lengths (Å)			
Cu1-Cl1	2.2802(9)	Cu1-N1	1.963(2)
Cu1-Cl1*	2.2802(9)	Cu1-N1*	1.963(2)
Bond angles (°)			
Cl1-Cu1-N1	89.65(7)	Cl1 -Cu1-Cl1*	180.00
Cl1-Cu1-N1*	90.35(7)	Cl1* -Cu1-N1	90.35(7)
N1-Cu1-N1*	180.00	Cl1*-Cu1-N1*	89.65(7)

Table 4.6. Bond distances and bond angles for the complex **3**

Bond lengths (Å)			
Cu1- N1	1.9625(19)	Cu1- O3*	2.003(2)
Cu1- N1*	1.9625(19)	Cu1- O5	2.612(2)
Cu1- O3	2.003(2)	Cu1- O5*	2.612(2)
Bond angles (°)			
O3-Cu1-O5	54.13(8)	O3-Cu1-O5*	125.87(8)
O3-Cu1-N1	89.73(8)	O3 -Cu1-N1*	90.28(8)

O3-Cu1-O3*	180.00	O5-Cu1-N1	79.79(8)
O3*-Cu1-O5	125.87(8)	N1-Cu1-N1*	180.00
O5-Cu1-O5*	180.00		
O5-Cu1-N1*	100.21(8)		

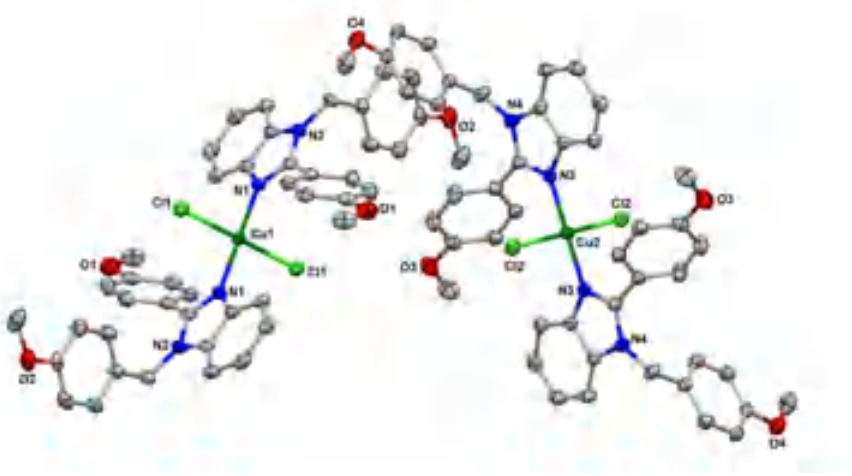

Fig. 4.7. Plot of the thermal ellipsoidal of **2** with 30% ellipsoid probability

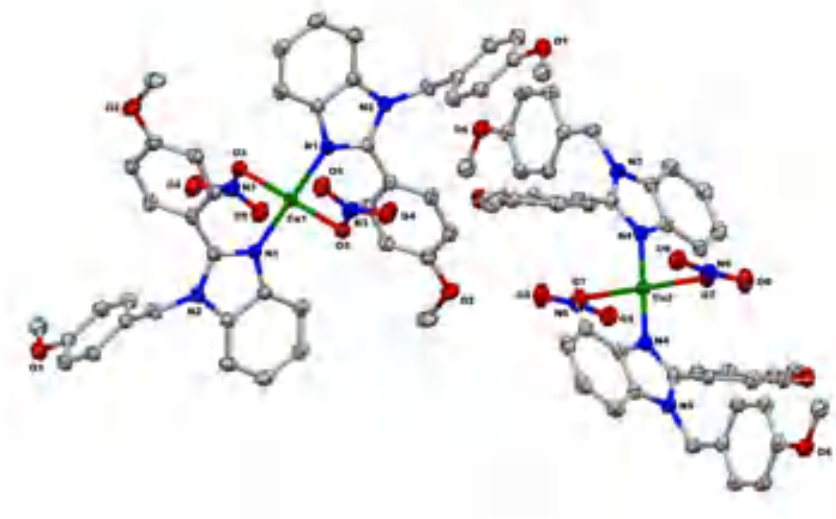

Fig. 4.8. Thermal ellipsoidal plot of **3** with 30% probability

In both cases, the coordinating atoms were in a trans-coordination environment. Analysis of bond angles Cl1-Cu1-N1 and Cl1-Cu1-N1* of 89.65(7)° and 90.35(7)° in **2** and N1-Cu1-O3 and O3-Cu1-N1* of 89.74(8)° and 90.26(8)° in **3** were almost 90° and existed in a perfect square planer geometry. The NO_3^- ligand coordinated through O3

atom in **3** was found in a proximal planer conformation with the uncoordinated O5-atom being in a *cis*-orientation relative to the copper(II) atom. This was also reflected in the Cu1-O3-N3-O5 torsion angle, which was slightly deviated from 0°. Monodentate coordination mode of both NO_3^- ligands in **3** was confirmed from the criteria listed in **Table 4.7**. All the values, Δd, $\Delta d'$, $\Delta\theta$, and θ_3 of 0.609 Å, 0.037 Å, 28.19°, and 119.30° respectively for **3** were in the range of monodentate coordination mode (**Table 4.7**).

Table 4.7. Criteria for assigning nitrate coordination modes

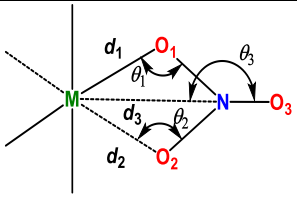

$\Delta d = d_1 - d_2$, $\Delta d' = d_3 - d_2$
$\Delta\theta = \theta_1 - \theta_2$

	Monodentate	Anisobidentate	Bidentate	Nitrate in **3**
Δd/Å	> 0.6	0.3-0.6	< 0.3	0.609
$\Delta d'$ /Å	< 0.1	0.14.2	> 0.2	0.037
$\Delta\theta$/°	> 28	14-28	< 14	28.19
θ_3 /°	< 162	162-168	> 168	119.30

The Cu-N bond lengths in the copper(II) complexes were the same, 1.963(2)Å (**Table 4.5** and **4.6**). Bond length analysis within the NO_3^- ligand showed a relatively long N3–O3 bond length of 1.265(3). The N3–O4 and N3–O5 bond lengths of 1.265(3) and 1.249(3), on the other hand, were relatively short. Therefore, a tendency toward localization of more negative charge on the coordinated O3 atom in contrast to the free NO_3^- anion could confirmed from this bond length analysis. Deviation from coplanarity of the benzimidazole and the para-methoxyphenyl rings, was given by the torsion angle (φ), N1–C8–C5–C4 in 1 and N1–C7–C8–C9 in **3** respectively (**Table 4.7**). It can be seen that the value of φ was increased from 36.7° in free $\mathbf{L^3}$ to 46.30° in **2** and 48.57° in **3**. The structures of **2** and **3** were very close as evident from the identical space group and crystal system, and the unit cell dimensions exhibited a very small difference in cell axes (**Table 4.4**).

4.3.6. Hirshfeld surface analysis

The nature of Hirshfeld surfaces of complexes **2** and **3** was analysed using d_{norm} calculation through Crystal Explorer software (**Fig. 4.9** and **4.10**). The d_{norm} area and the area consisting of supramolecular interactions of the complexes **2** and **3** with their neighbouring units were displayed in red colour. The 2D fingerprint plots and elemental participation in % share of close interaction with others were displayed in **Fig. 4.11** and **4.12** respectively. In the d_{norm}, blue areas were showing the engagement of π···π

interactions between phenyl centroid of the ligand while red area highlights intermolecular C-H···O/Cl/N interactions and displays in Fingerprint plots (**Fig. 4.11** and **4.12**). It was also observed that the self-assembled supramolecular architectures for complex **2** were principally dominated by C-H···O/Cl interactions (**Fig. 4.13**) whereas the self-assembled 3D network for complex **3** was constructed by C-H···O interactions (**Fig. 4.14**). The H···O/Cl interactions were found of moderate strength (2.42-2.56 Å; **Table 4.8**) in **2** however extensive but moderate to weak ranged H···O interactions were noted in the construction of the supramolecular architecture of complex **3** (2.42-2.56 Å; **Table 4.9**).

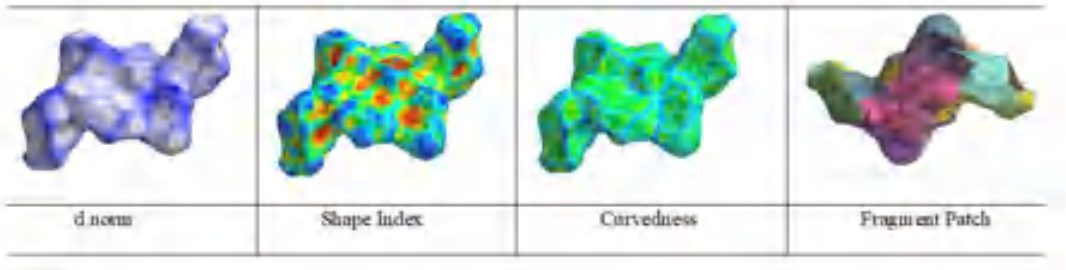

Fig. 4.9. Hirshfeld surface of **2**

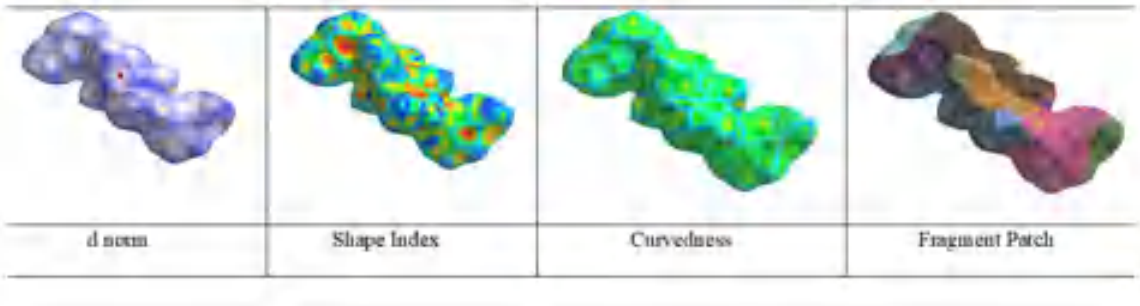

Fig. 4.10. Hirshfeld surface of **3**

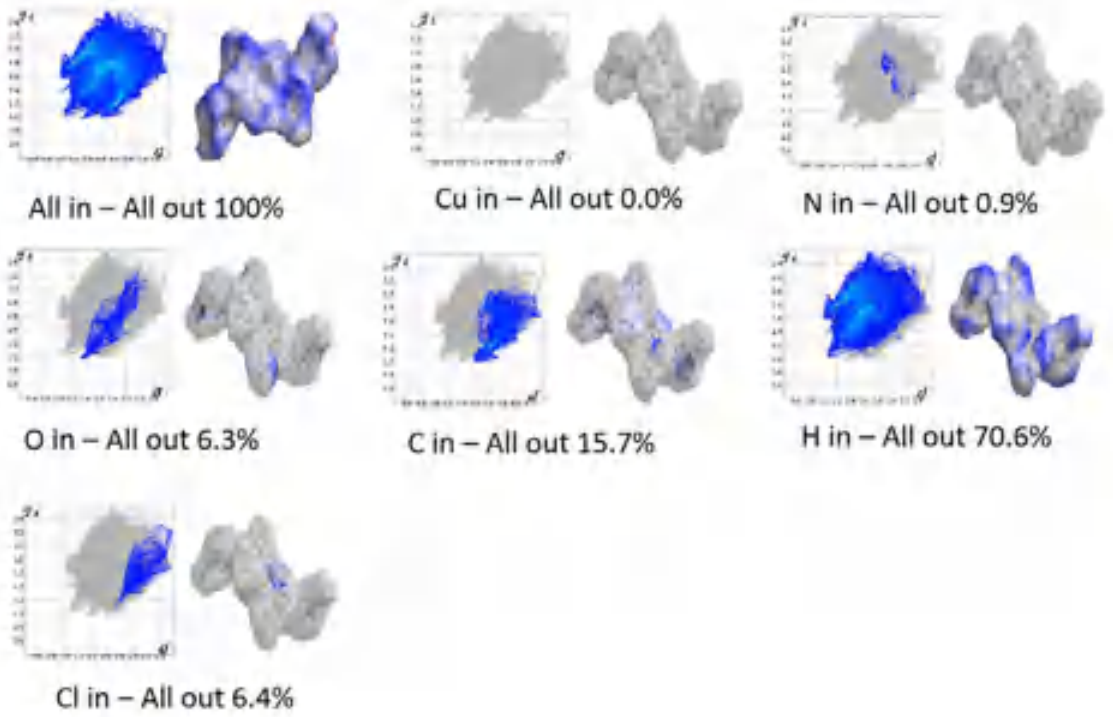

Fig. 4.11. 2D finger print plots of complex **2**. (a) All inside-X(Cu,N,O,C,H,Cl) outside

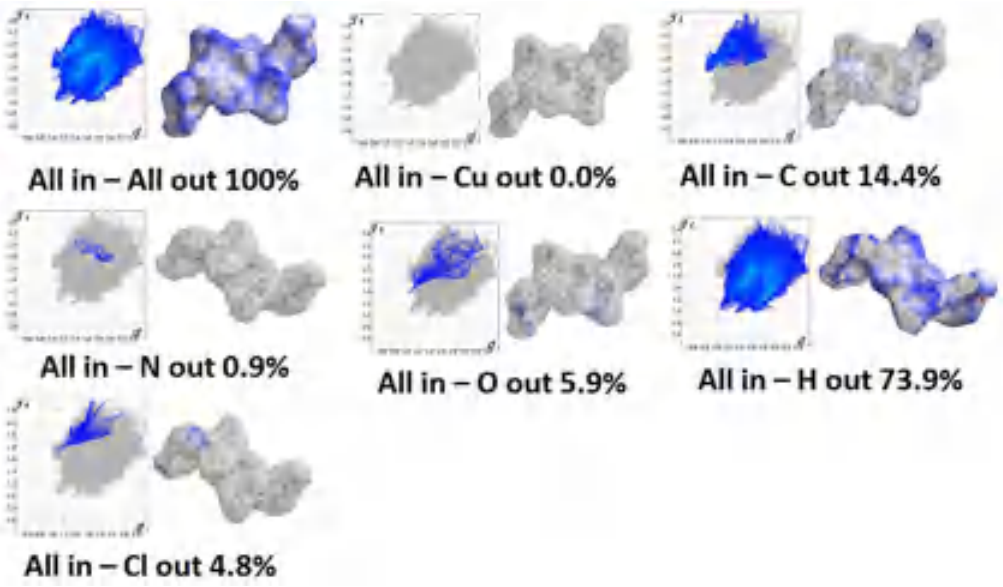

Fig. 4.11. 2D finger print plots of complex **2**; (b)All outside - X(Cu,N,O,C,H,Cl) inside

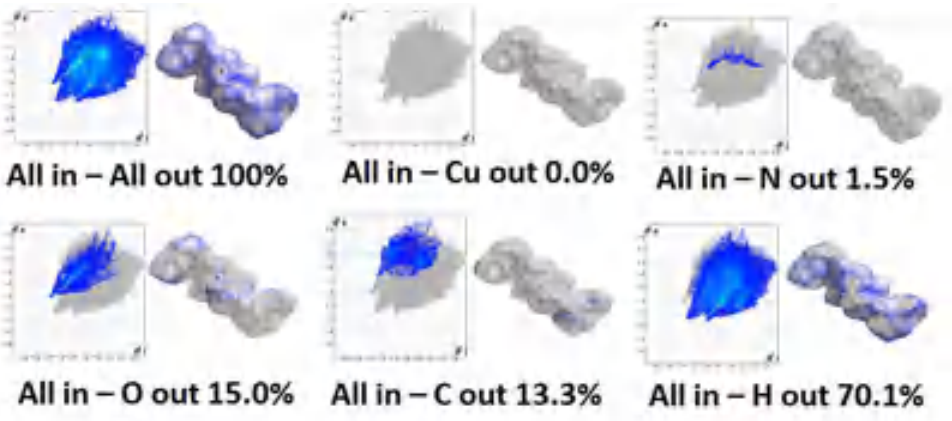

Fig. 4.12. 2D finger print plots of complex **3**. (a) All inside-X (Cu,N,O,C,H) outside

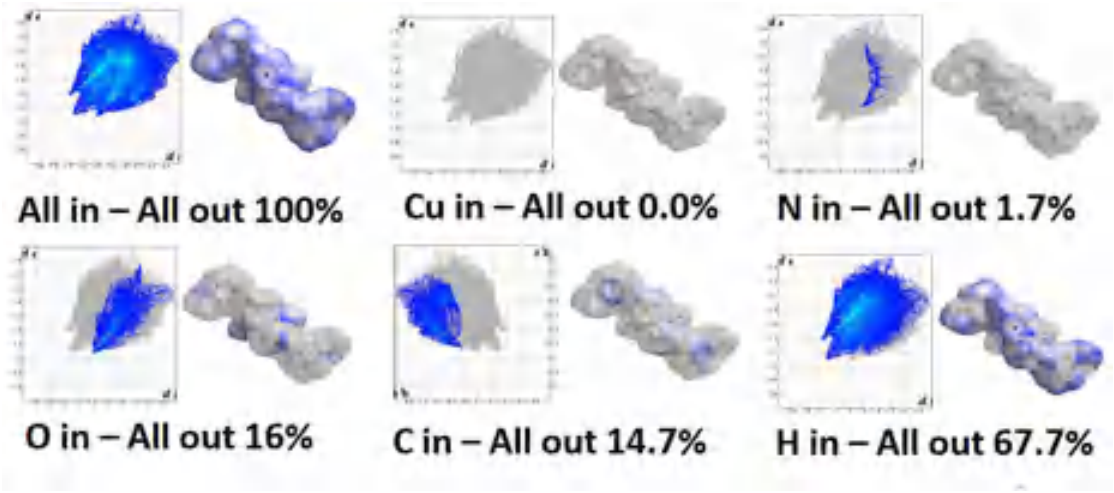

Fig. 4.12. 2D finger print plots of complex **3**. (b) All outside -X (Cu,N,O,C,H) inside

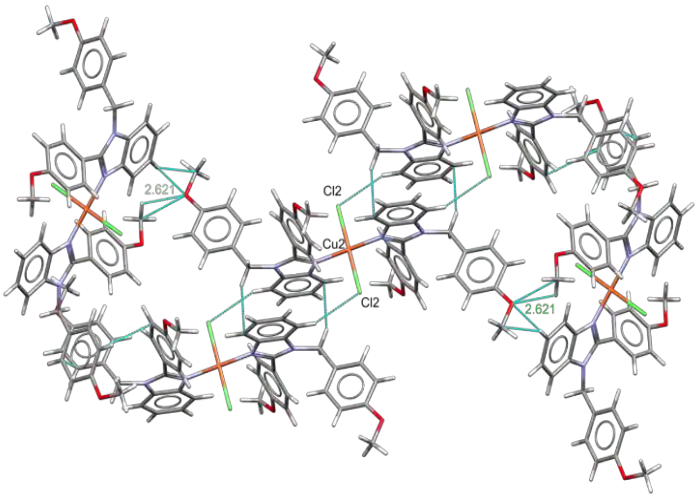

Fig. 4.13. H···Cl and H···O interaction-based construction of 3D architecture for complex **2**

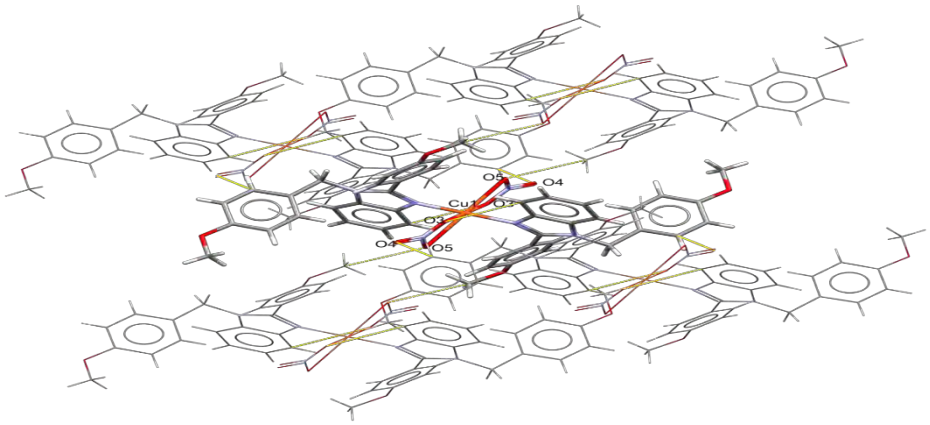

Fig. 4.14. H···Cl and H···O interactions based construction of 3D architecture for complex **3**

Table 4.8. Hydrogen bond parameters donor/acceptor scheme (Å,°) for copper complex**2**

D-H…A	D-H	H…A	D…A	D-H…A	Symmetry code
C13-H13…Cl1	0.950	2.87	3.846	150	x-1,+y,+z
C35-H35…Cl2	0.950	2.921	3.799	154	-x+1,-y+1,-z+1
C33-H33…O2	0.950	2.562	3.433	152	-x,-y+1,-z-x+1,-y+1,z+1
C11-H11…O4	0.950	2.427	3.320	145	-x+1,-y+1,-z

Table 4.9. Hydrogen bond parameters donor/acceptor scheme (Å,°) for copper complex **3**

D-H…A	D-H	H…A	D…A	D-H…A	Symmetry code
C12-H12…O8	0.930	2.631	3.521	160	x, y, z
C34-H34…O4	0.930	2.649	3.517	155	x, y, z
C9-H9…O5	0.930	2.503	3.306	144	-x+2,-y+2,-z
C31-H31…O9	0.930	2.514	3.324	146	-x+2,-y+2,-z+1
C4-H4…O6	0.930	2.540	3.391	152	-x+1,-y+2,-z
C26-H26…O1	0.930	2.629	3.481	153	-x+1,-y+2,-z+1
C14-H14B…O4	0.930	2.598	3.380	139	x,+y+1,+z

4.3.7. Catalytic oxidation studies of 2-aminophenol and mechanistic inferences

The catalytic oxidation of 2-aminophenol (2-AP) was studied with the copper(II) complexes. In the course of oxidation reaction, 2-aminophenol (2-AP) was considered as a standard substrate in methanol (**Scheme 4.3**). The bio-mimics of catalytic oxidation of 2-AP were monitored with a spectrophotometer at an interval of 8 min for 2h. It is well documented that 2-AP exhibited a single band at 267
nm. Upon addition of copper(II) complexes (1×10^{-4} M solution) to 2-AP (1×10^{-2} M solution), the appearance of new electronic bands at 433 and 430 nm with increasing intensity was observed for both **2** and **3** respectively (**Fig. 4.15** and **4.16**).

Scheme 4.3. Oxidative coupling of 2-aminophenol by phenoxazinone synthase

The development of the electronic bands at 433 and 430 nm for **2** and **3** was a signature for the production of phenoxazinone compound in solution which was well established in the scientific literature.[57,58] Controlled experiments were also performed using 2-AP and 2-AP in presence of benzimidazole functionalized ligand $\mathbf{L^3}$ separately under an identical reaction conditions (**Fig. 4.17**) up to 2h, however, yields of control reactions were very little and can be ignored. The production of oxidation product in control reactions revealed that auto-oxidation of 2-AP under ambient reaction condition.

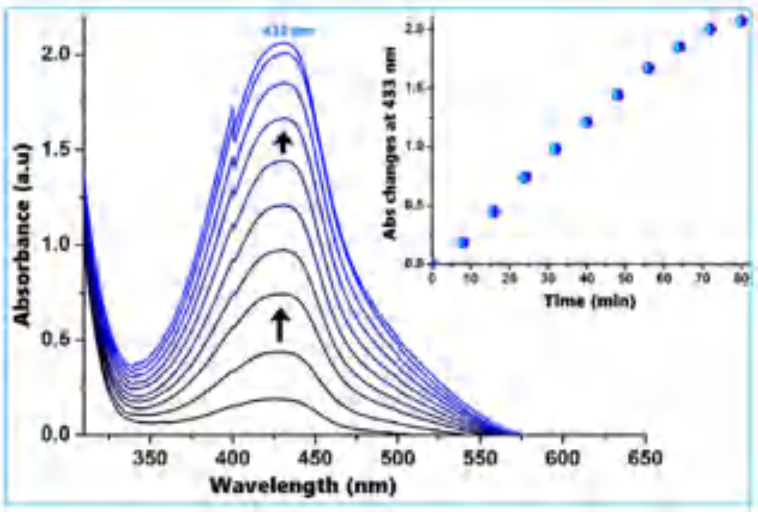

Fig. 4.15. Generation of a new electronic band at 433 nm after addition complex **2** to 2-AP in MeOH with a time interval of 8 mins. Inset: Time vs Absorbance plot at 433 nm

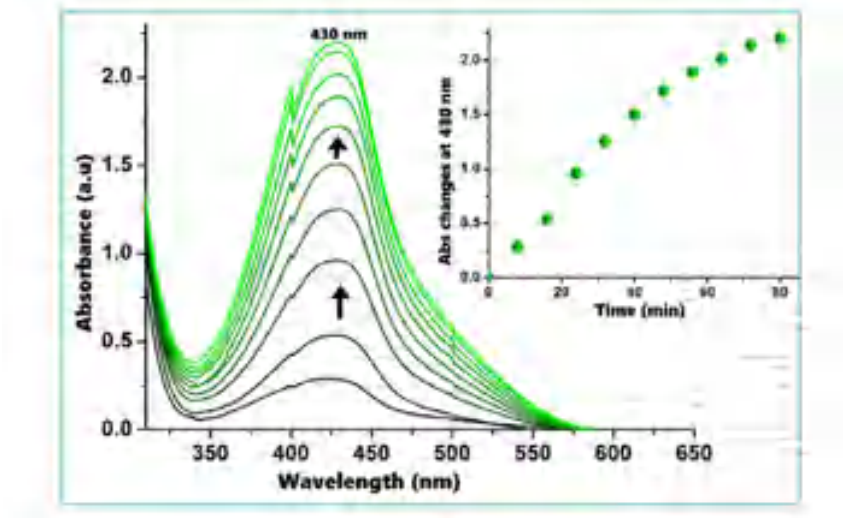

Fig. 4.16. Development of a new electronic band at 430 nm after treatment of complex **3** to 2-AP in MeOH with a time interval of 8 mins. Inset: Time vs Absorbance plot at 430 nm

The phenoxazinone species was extracted by column chromatographic method. Neutral alumina as column support and benzene-ethyl acetate as an eluant mixture were employed for this chromatographic separation. The oxidation product was isolated in high yield (~83% & ~76% for **2** & **3**). The product was principally identified by ^{1}H NMR spectroscopy. [42,52,57] ^{1}H NMR data for 2-amino-3*H*-phenoxazine-3-one (APX), ($CDCl_3$, 400 MHz,) ^{1}H: 7.61 (m, 1H), 7.46 (m, 3H), 6.48 (s, 1H), 6.39 (s, 1H), 6.27 (s, 1H).

Kinetic studies of the catalytic oxidation of 2-AP were carried out to understand the catalytic efficacy for the copper(II) complexes. The method of initial rates was followed to unveil the nature of kinetic for this catalytic oxidation of 2-AP. The kinetics of oxidative coupling of 2-AP was monitored for the growth of oxidized products at 433 and 430 nm as a function of time (**Fig. 4.18** and **4.19**). [59-62] The rate constants vs. concentration of the substrate plot seem to be saturation kinetics. The values of the kinetics parameters for the oxidation of 2-AP by **2** and **3** were determined considering the Michaelis−Menten approach of enzymatic kinetics and summarized in **Table 4.10**. An attempt was also made to examine the reactivity of the synthesized copper complexes with a comparison of the kinetic parameter for other reported copper complexes. [5,42,52,55,63-65]

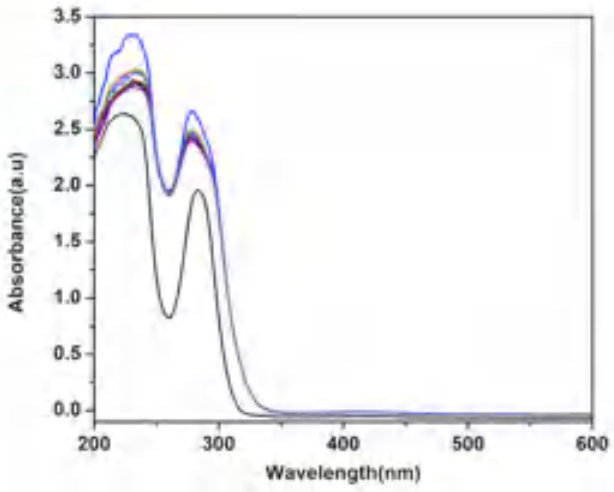

Fig. 4.17. Controlled experiment using catalytic amount of benzimidazole ligand to 2-AP under identical reaction conditions

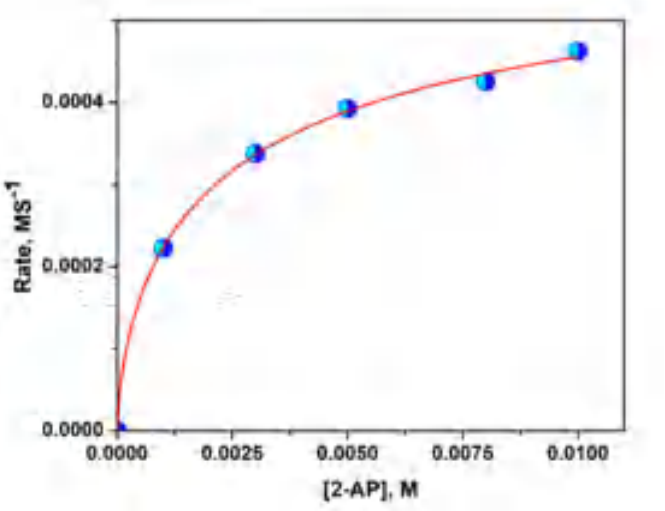

Fig. 4.18. Plot of rate of reaction vs [2-AP] for the catalytic oxidation of 2-AP by **2**

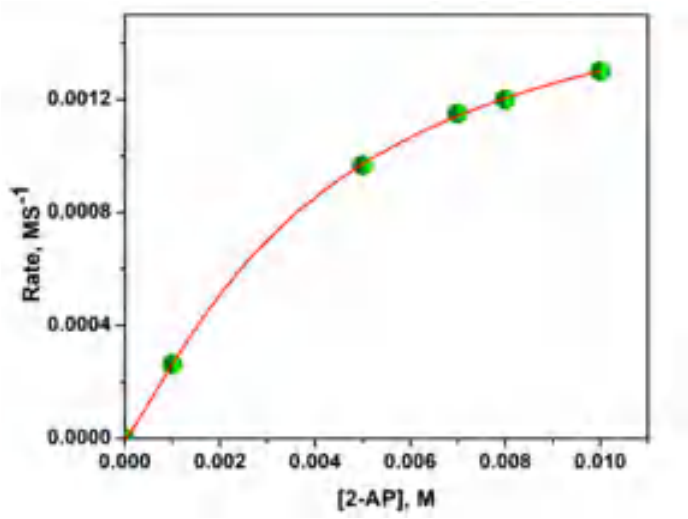

Fig. 4.19. Plot of rate of reaction vs [2-AP] for the catalytic oxidation of 2-AP by **3**

Table 4.10. Comparison of k_{cat} (h^{-1}) values for catalytic oxidation of 2-AP by reported copper(II) compounds and copper complexes **2** and **3**

Complex	k_{cat} (h^{-1})(Solvent)	CCDC No	Ref
$[L^1Cu(\mu\text{-}Cl)_2CuL^1]$	1.06×10^4 (CH_3OH)	1572023	[63]
$[Cu_4(L^2)_4]$	86.3 (CH_3OH)	1507035	[64]
$[Cu_4(L^3)_4]$	340.26 (CH_3OH)	1507036	[64]
[Cu(μ-Cl)(Phen)Cl]	1.69×10^4(CH_3OH)	1524680	[52]
$[(CH_3CN)Cu(L_s)_2Cu]^{2+}$	11.1 (CH_3OH)	1940162	[65]
$[Cu_2(L^{b1})_3]ClO_4$	78.14 (CH_3CN)	1957033	[42]
$[Cu(L^{b2})_2]$	536.4 (CH_3CN)	2024056	[5]
$[Cu(L^{b3})](H_2O)$	5.89×10^2 (CH_3OH)	1981345	[61]
$[Cu(\mathbf{L^3})_2Cl_2]_2$ (**2**)	2.31×10^4 (CH_3OH)	2046275	This work
$[Cu(\mathbf{L^3})_2(NO_3)_2]_2$ (**3**)	6.3×10^4 (CH_3OH)	2046276	This work

L^1 = 2-(a-Hydroxyethyl)benzimidazole (Hhebmz), L^2 = (E)-4-Chloro-2-((thiazol-2-ylimino)methyl)phenol, L^3 = (E)-4-Bromo-2-((thiazol-2-ylimino)methyl)phenol, L^{b1} = (Z)-2-methoxy-6-(((2-methoxyphenyl)imino)methyl)phenol, L^{b2} = 2-(2-methoxybenzylideneamino) phenol,

Michaelis–Menten equation is presented as:

$$V = \frac{V_{max}\,[S]}{K_M + [S]}$$

Where, V indicates the reaction rate, K_M was considered as the Michaelis–Menten constant, V_{max} presents maximum reaction velocity, and [S] was the substrate concentration.

The values of kinetics parameters were determined from Michaelis−Menten approach of enzymatic kinetics for **2** as $V_{max}(MS^{-1}) = 6.44\times10^{-4}$; $K_M = 2.63\times10^{-3}$ [Std. Error for V_{max} $(MS^{-1}) = 7.65\times10^{-5}$; Std. Error for K_M (M)= 1.29×10^{-4}] and for **3** as $V_{max}(MS^{-1}) = 1.75\times10^{-3}$; $K_M = 4.18\times10^{-3}$ [Std. Error for V_{max} $(MS^{-1}) = 4.16\times10^{-5}$; Std. Error for K_M (M)= 1.97×10^{-4}].

The turnover number (k_{cat}) for the copper(II) complexes **2** and **3** were determined as 2.31×10^4 and 6.3×10^4 h^{-1} respectively. The catalytic efficiency (k_{cat}/K_M) for **2** and **3** towards phenoxazinone synthase activity was found high and calculated as 8.78×10^6 and 1.50×10^7. It was observed that complex **3** exhibited ~2 fold greater rate of oxidation compare to complex **2**. In the copper(II) complex **3**, the presence of coordinated nitrate with Cu(II) centre creates higher steric hindrance and leads to more lability, and as a consequence loss of the coordinated nitrate probably occurs during the incoming approach of 2-AP towards the copper(II) centre. For complex **3**, the presence of coordinated chloride to the square plane of Cu(II) centre facilitates a more stable/inert structure compared to **2**. The high catalytic efficiencies of the copper(II) complexes may be explained from the perspective of easy incorporation of 2-AP through the expansion of the coordination number of copper(II) centres. The higher rate of catalytic oxidation for complex 3 was further evaluated in terms of determination of the activation parameters obtained from Eyring equation/Arrhenius equation through temperature dependent kinetic measurements. To understand the thermal effect on the rate of catalytic oxidative coupling of 2-AP, kinetic experiments were carried out with both the complexes in the temperatures range (283K – 303K). During the kinetic measurement at different temperature, the concentration for both the copper complexes was kept constant as 1×10^{-3} M while the concentration of 2-AP was fixed at 1×10^{-2} M. It was observed that the rate of oxidation of 2-AP increases with increase in temperature for both the copper(II) complex catalysed reactions. The activation energy (E_a), heat of enthalpy ($\Delta H^{\ddagger}$), and entropy change ($\Delta S^{\ddagger}$) (**Table 4.11**) were determined from the Arrhenius (**Fig. 4.20**) and Eyring (**Fig. 4.21**) plots. The activation energy for the complex **3** catalysed oxidation of 2-AP was found 9.67 kJ mol^{-1} which was lower than that of complex **2** (E_a = 25.68 kJ mol^{-1}). Noteworthy, both the complexes exhibit negative $\Delta S^{\ddagger}$ value and recommends the formation of substrate-complex adduct at the transition state.

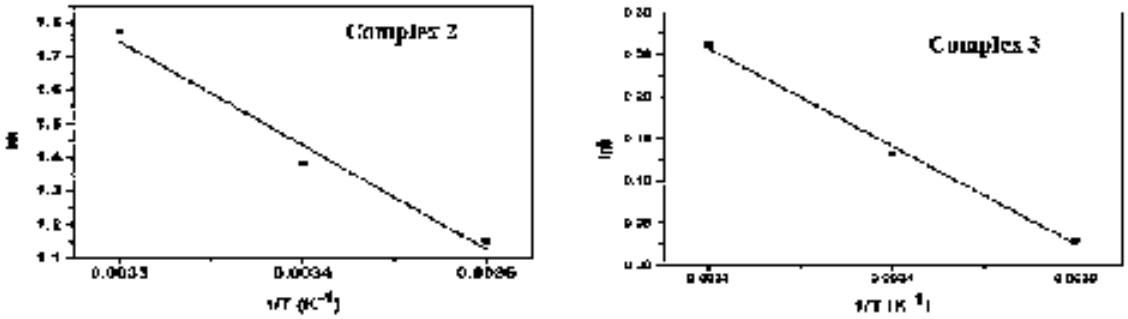

Fig. 4.20. Arrhenius plot of for the catalytic oxidation of 2-AP by **2** and **3**

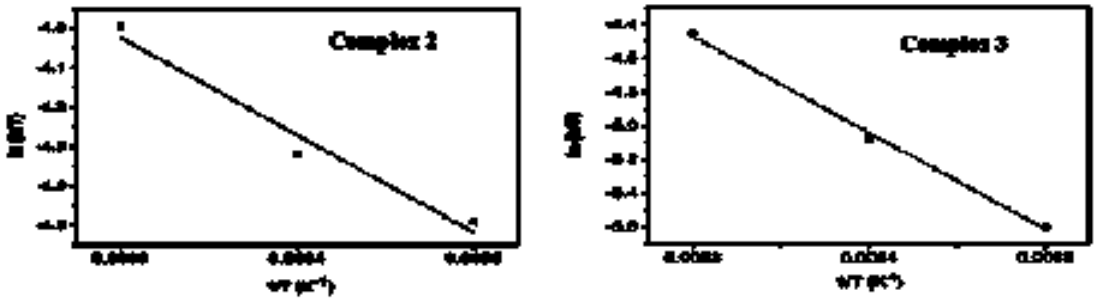

Fig. 4.21. Eyring plot of for the catalytic oxidation of 2-AP by **2** and **3**

Table 4.11. Activation parameters for the aerial oxidation of 2-AP by the copper(II) complexes

Complexes	E_a (kJ mol^{-1})	$\Delta H^{\neq}$ (kJ mol^{-1})	$\Delta S^{\neq}$(J mol^{-1} K^{-1})
Copper Complex 2	25.68	20.5688	-163.1038
Copper Complex 3	9.6775	48.4083	-74.9964

The redox activities of copper(II) complexes and mixtures of the complexes with 2-AP were studied by cyclic voltammetry in CH_2Cl_2. The electrochemical potential values corresponding to active species of the copper complexes with reference to ferrocenium/ferrocene (Fc^+/Fc) couple are displayed in **Table 4.12**. The cyclic voltammograms for complexes **2** and **3** were illustrated in **Fig. 4.22 and Fig. 4.23**. Both the copper complexes produce quite similar nature of cathodic and anodic waves in the presence and absence of 2-AP. Complexes **2** and **3** showed reversible cathodic waves at -0.655 V and -0.730 V which may be assigned as imine/imine anion radical corresponding to $2e^-$ redox waves of the two C=N bonds in two benzimidazole ligands.

The other cathodic peaks at -1.53 V and 1.68 V for complexes **2** and **3** appear for the irreversible Cu^{2+}/Cu^{+} redox couples.

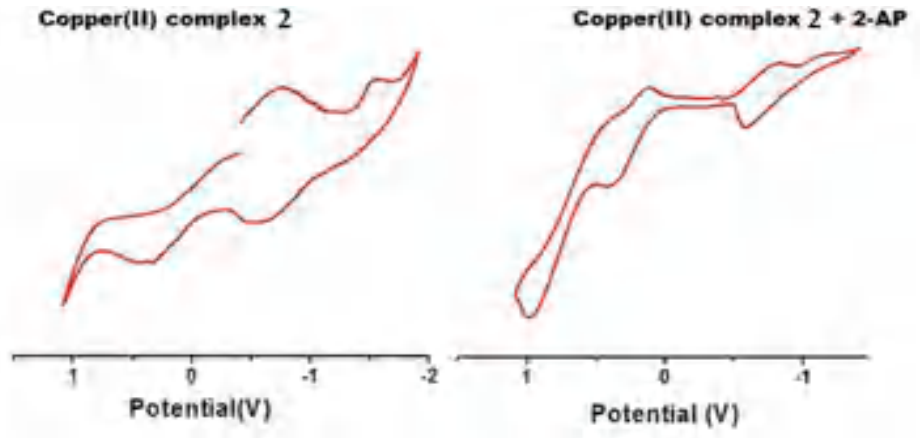

Fig. 4.22. Left: Cyclic voltammogram of the copper complex **2** in anhydrous DCM medium; **Right:** Cyclic voltammogram of copper complex **2** in presence of 2-AP under molecular oxygen atmosphere in anhydrous DCM in CH_2Cl_2 (0.20 M $[N(n{-}Bu)_4]PF_6$) at 295 K

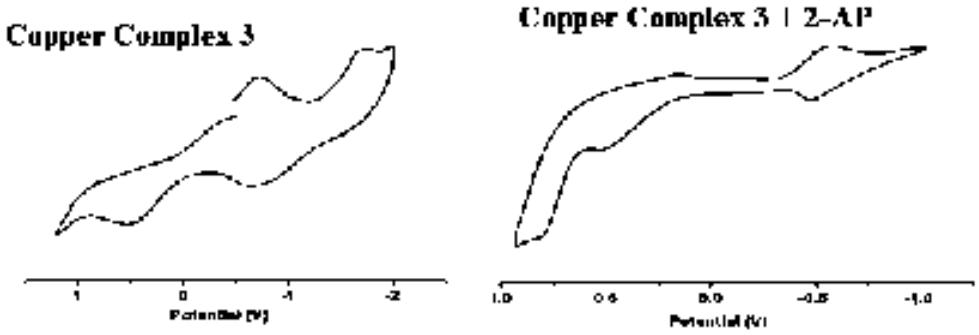

Fig. 4.23. Left: Cyclic voltammogram of the copper complex **3** in anhydrous DCM medium; **Right:** Cyclic voltammogram of copper complex **3** in presence of 2-AP under molecular oxygen atmosphere in anhydrous DCM in CH_2Cl_2 (0.20 M $[N(n{-}Bu)_4]PF_6$) at 295K

The copper complexes **2** and **3** showed the presence of anodic peaks at 0.38 V and +0.52 V respectively. In the mixture of individual copper complexes, **2** and **3** in presence of 2-AP, the reversible cathodic wave of imine/imineanion radical shifted to -0.68 V and -0.97 V respectively. Noteworthy, the irreversible cathodic peak of Cu^{2+}/Cu^{+} redox couple in **2** shifted to -1.14 V. In addition to the presence of cathodic waves, each of the copper complexes exhibited reversible anodic waves at +0.25 V and +0.48 V respectively and suggests the development of 2-AP^{-}/ 2-$AP^{\bullet-}$ redox couples in the course of catalysis. An irreversible anodic peak at +0.98 V for complex **2** in presence of 2-AP

was also observed and may be attributed to the presence of 2-AP$^{\bullet-}$/2-IQ redox couple in solution. The electrode potential values observed for the development of 2-AP$^{\bullet-}$/2-IQ species in the course of catalytic oxidation of 2-AP were well corroborated with the values reported by a few previously reported copper complexes. [5,42,55]

Table 4.12. Redox potentials data of the copper complexes in presence and absence of 2-AP determined by cyclic voltammetry in CH_2Cl_2 (0.20 M $[N(n-Bu)_4]PF_6$) at 295 K

Compounds	$E_{1/2}$[1] (V) (ΔE^a, mV)	$E_{½}$[2],V (ΔE^a, mV)
2	+0.38[b]	-0.655 (150), -1.53[c]
2 +2-AP	+0.25 (200), +0.98[b]	-0.68 (160), -1.14[c]
3	+0.52	-0.730, -1.68
3 +2-AP	+0.48	-0.97
[a]peak to peak separation in mV, [b]anodic peak [c]cathodic peak		

To find further insights into the mechanistic aspects of the course of catalysis, X-band EPR spectral analysis of the reaction mixture of copper complex **2** with 2-AP was carried out in DCM medium. Complex **2** produces four line hyperfine EPR spectra (**Fig. 4.24**) for the presence of ^{63}Cu (I= 3/2) and the g value was found 2.116 which may be well correlated with the reported EPR spectra of copper(II) ion.[5,42] However, when 2-AP was added to the complex **2** solution, the hyperfine spectra was quenched and a new single line spectra was found at g= 2.001 indicating the presence of iminobenzoquinone radical (**Fig. 4.25**).[5]

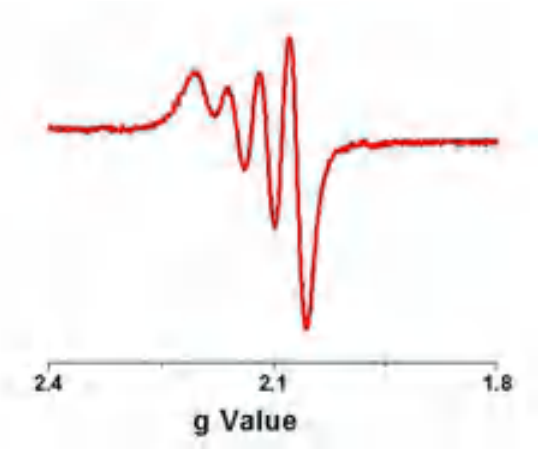

Fig. 4.24. EPR spectrum of complex **2** in DCM medium

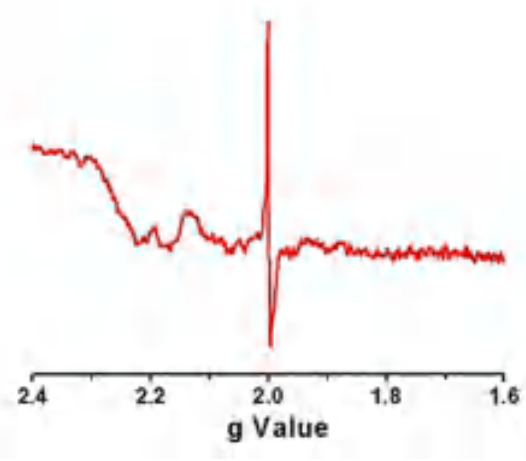

Fig. 4.25. EPR spectrum of the complex **2** in presence of 2-AP anhydrous DCM medium

Furthermore, electrospray ionization (ESI) mass spectra of the copper(II) complexes **2** and **3** in presence of 2-AP were measured after mixing of 10 mins to understand the labile character and the binding aspects of the copper(II) complexes with 2-AP in MeOH medium. The spectra are shown in **Fig. 4.26** and **Fig. 4.27** for complexes **2** and **3** respectively. It was observed that the ESI-MS of the reaction mixture for **2** (**Fig. 4.26**) showed a base peak at m/z 213.27 which was attributed to the existence [(2-amino-3*H*-phenoxazine-3-ones)+H^+] species in solution. Furthermore, a characteristics peak at m/z 823.55 was also detected which reveals the presence of molecular ion peak. The binding adduct between complex **2** and 2-AP, [[**1**+(2-AP)]+H^+] was further confirmed from the appearance of another characteristic peak at 927.41 m/z. ESI-MS spectrum of complex **3** with 2-AP (**Fig. 4.27**) displayed a characteristic peak at 213.29 and confirmed the development of [(2-amino-3*H*-phenoxazine-3-ones)+H^+] species in MeOH. The enzyme-substrate adduct for complex **3** was also ensured as [[Cu($\mathbf{L^3}$)$_2$+(2-AP)]+H^+] which corroborated well with the characteristic peak at m/z 860.29 in the spectrum. However, the molecular ion peak for complex **3** was absent in the spectrum. Therefore, ESI-MS spectra for both the copper complexes suggest that both the complexes undergo the course of catalysis through the formation of the enzyme-substrate adduct. It was also recommended that complex **3** in addition to 2-AP displaced the coordinated nitrates to the solution and more lability or coordinatively unsaturation at the copper(II) centre facilitates higher catalytic performance than complex **2**. The participation of aerobic oxygen was also examined to understand the fate of O_2 through the detection of hydrogen peroxide in the course of catalysis. The development of hydrogen peroxide was detected with a UV-Vis spectrophotometer and the observed electronic band at 353

nm corresponds to the production of I_3^- species (**Fig. 4.28**)[55] and thereby, confirmed the existence of hydrogen peroxide. Therefore, based on spectrophotometric, kinetics, ESI-MS spectra of the reaction mixtures, electrochemical analysis, and EPR spectral measurement, the mechanistic pathways for the course of catalytic oxidation may be proposed according to **scheme 4.4**.

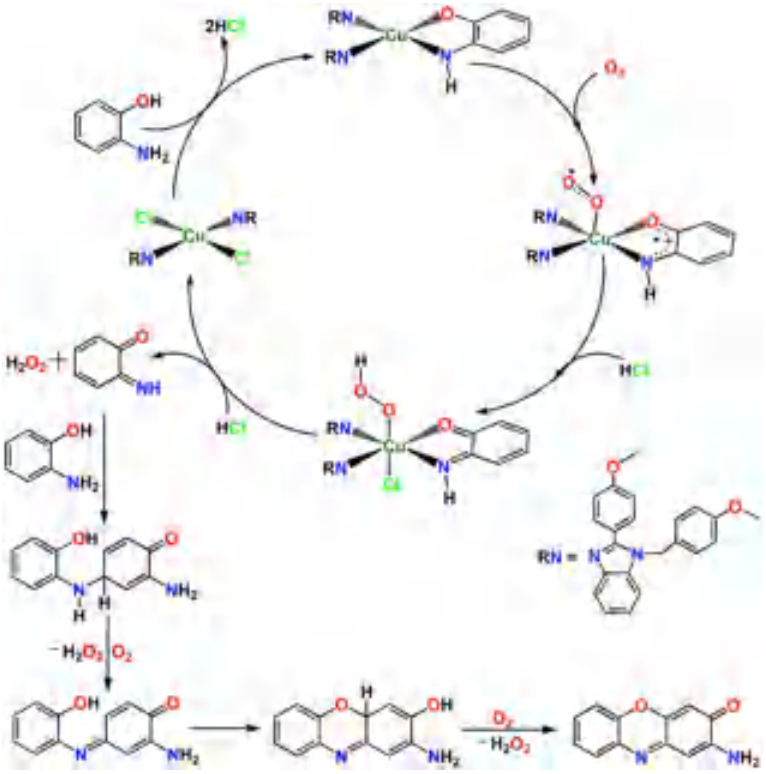

Scheme 4.4. Plausible mechanistic pathway for phenoxazinone synthase activity of the copper complexes

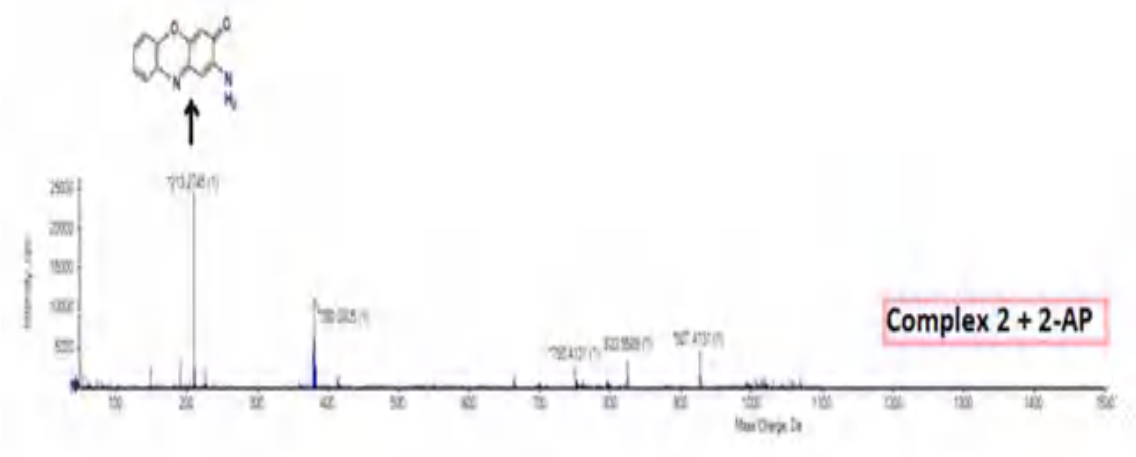

Fig. 4.26. ESI-MS spectrum of complex **2** in presence of 2-AP in MeOH

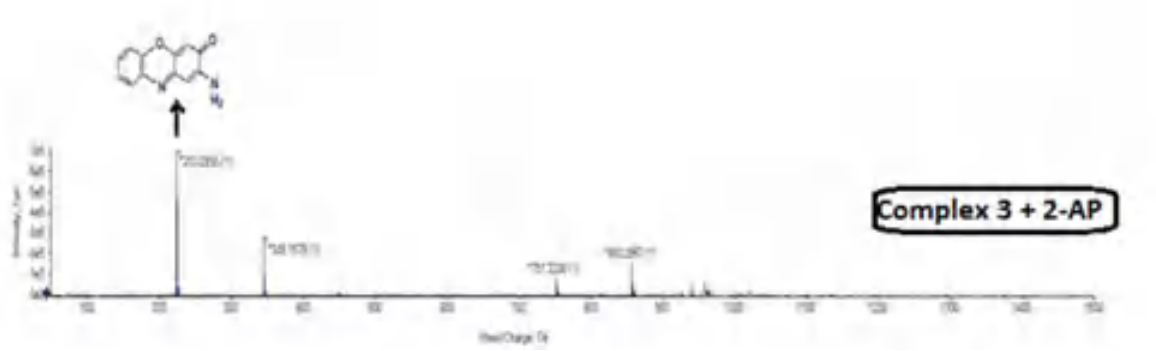

Fig. 4.27. ESI-MS spectrum of complex **3** in presence of 2-AP in MeOH

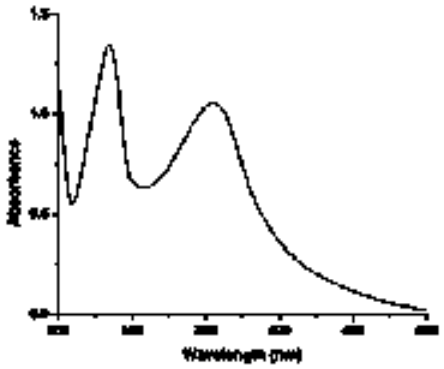

Fig. 4.28. Absorbance profile of I_3^-

4.4. Conclusions

This research study reported the details of synthesis, spectroscopic, and structural characterization of a newly designed substituted benzimidazole ligand and two structurally similar copper(II) complexes containing the ligand. The effect of ancillary ligands (chloride and nitrate) in the bio-mimics of phenoxazinone synthase activity has also been investigated. X-ray structural analysis exhibited that both the complex adopts a perfect square planar geometry and exists in *trans* configuration. It was observed that the catalytic efficiency (k_{cat}/K_M) for both the copper complexes was found high towards the bio-mimicking oxidation of 2-AP. k_{cat}/K_M values were determined as 8.78×10^6 and 1.50×10^7 for **2** and **3** respectively and it can be addressed that the catalytic oxidation efficiency was almost double that of **2**. The presence of coordinated nitrate in **3** creates steric repulsion in the square plane and made the complex more labile which facilitates the entrance of 2-AP to the Cu(II) centre. Electrochemical analysis for both the copper complexes in presence of 2-AP confirms the development of AP^-/ $AP^{\bullet-}$ redox couple in the course of oxidative coupling of 2-AP. EPR spectral analysis consolidates the

existence of organic radical at g=2.01 and supports the catalytic oxidation as radical driven. The evaluated activation parameters through temperature-dependent kinetic measurements further supports the higher rate of catalytic oxidation of 2-AP for complex **3**. Finally, this study led to easy preparation of benzimidazole derivative ligand and its copper(II) complexes and explores the effect of ancillary ligands in the bio-mimetic oxidation of 2-AP through details spectroscopic, ESI-MS, and electrochemical methods.

References

[1]. T. Shi, Y. Xu, Y. J. Zou and Z. X. Wang, *Dalton Trans*., 2019, **48**, 11186-11190.

[2]. P. Xiao, F. Dumur, J. Zhang, J. P. Fouassier, D. Gigmes and J. Lalevée, *Macromolecules*, 2014, **47** (**12**), 3837–3844.

[3]. M. Mondal, S. Jana, M. G. B. Drew and A Ghosh, *Polymer*, 2020, **204**, 122815.

[4]. S. Dasgupta, G. Aullón, E. Zangrando, D. Das, *New J. Chem*., 2019, **43**, 2501-2512.

[5]. S. Mahato, N. Meheta, K. Muddukrishnaiah, M. Joshi, P. Ghosh, M. Shit, A. R. Choudhury and B. Biswas, *Appl. Organomet. Chem*., 2020, **34**, e5935.

[6]. K. A. Magnus, H. T. That and J. E. Carpenter, *Chem. Rev*., 1994, **94**, 727.

[7]. A. S. Ferrer, J. N. R. Lopez, F. G. Canovas, F. G. Carmona, *Biochim. Biophys. Acta*., 1995, **1**, 1247.

[8]. C. Gerdemann, C. Eicken and B. Krebs, *Acc. Chem. Res*., 2002, **35**, 183.

[9]. F. Fusetti, K. H. Schro¨ter, R. A. Steiner, P.I. van Noort, T. Pijning, H. J. Rozeboom, K. H. Kalk, M. R. Egmond and B. W. Dijkstra, *Structure*, 2002, **10**, 259.

[10]. R. A. Steiner, I. M. Kooter and B. W. Dijkstra, *Biochemistry*, 2002, **41**, 7955.

[11]. I. M. Kooter, R. A. Steiner, B. W. Dijkstra, P. I. van Noort, M. R. Egmund and M. Huber, *Eur. J. Biochem*., 2002, **269**, 2971.

[12]. J. W. Whittaker, *Chem. Rev*., 2003, **103**, 2347.

[13]. M. Halcrow, S. Phillips and P. Knowles, In Subcellular Biochemistry, **35**, Enzyme-*Catalyzed Electron and Radical Transfer*; A. Holzenburg, N.S. Scrutton, Eds.; Plenum: New York, 2000, **183**.

[14]. M. M. Whittaker, P. J. Kersten, N. Nakamura, J. S. Loehr, E. S. Schweizer and J. W. Whittaker, *J. Biol. Chem*., 1996, **271**, 681.

[15]. M. M. Whittaker, P. J. Kersten, D. Cullen and J. W. Whittaker, *J. Biol. Chem*., 1999, **274**, 36226.

[16]. H. H. T. Nguyen, K. H. Nakagawa, B. Hedman, S. J. Eliot, M. E. Lidstrom, K. O. Hodgson and S. I. Chan, *J. Am. Chem., Soc*., 1996, **118**, 12766.

[17]. S. J. Elliott, D. W. Randall, R. D. Britt and S. I. Chan, *J. Am. Chem. Soc*., 1998, **120**, 3247.

[18]. R. L. Lieberman, D. B. Shrestha, P. E. Doan, B. M. Hoffman, T. L. Stemmler and A. C. Rosenzweig, *Proc. Natl. Acad. Sci*., 2003, **100**, 3820.

[19]. E. Katz, 1967 *Biosynthesis of secondary metabolites: roles of trace metals Antibiotics II* (Gottlieb D, & Shaw P.D, Eds.) p 276, Springer, New York.

[20]. U. Hollstein, *Chem. Rev*., 1974, **74**, 625.

[21]. L. I. Simandi, S. Nemeth and N. Rumlis, *J. Mol. Catal*., 1987, **42**, 357.

[22]. A. Butenandt, *Angew. Chem*., 1957, **69**, 16.

[23]. T. M. Simándi, L. I. Simándi, M. Győr, A. Rockenbauer and A. Gömöry, *Dalton Trans*., 2004, 1056-1060.

[24]. G. W. K. Cavill, P. S. Clezy, J. R. Tetaz and R. L. Werner, *Tetrahedron*, 1959, **5**, 275.

[25]. J. Kaizer, R. Csonka and G. Speier, *J. Mol. Catal. A: Chem*., 2002, **180**, 91.

[26]. K. Ansari and C. Lal, *Eur. J. Med. Chem*., 2009, **44**, 2294–2299.

[27]. R. V. Devivar, E. Kawashima, G. R. Revankar, J. M. Breitenbach, E. D. Kreske, J. C. Drach and L. B. Townsend, *J. Med. Chem*., 1994, **37**, *18*, 2942–2949.

[28]. P. Keller, C. Müller, I. Engelhardt, E. Hiller, K. Lemuth, H. Eickhoff, K. H. Wiesmüller, A. B. Kentischer, F. Bracher and S. Rupp, *Antimicrob Agents Chemother*, 2015, **59(10)**, 6296-6307.

[29]. A. Hussain, M. F. AlAjmi, Md. T. Rehman, S. Amir, F. M. Husain, A. Alsalme, M. A. Siddiqui, A. A. AlKhedhairy and R. A. Khan, *Scientific Rep*., 2019, **9**, 5237.

[30]. A. Katiyar, J. Rai, S. Gangwar, A. K. Mohanty and A. P. Mishra, *J. Drug Discov. Dev*., 2018, **2**, 2–10.

[31]. M. J. Van Oosten, S. Silletti, G. Guida, V. Cirillo, E. Di Stasio, P. Carillo, P. Woodrow, A. Maggio and G. Raimondi, *Front. Recent Dev. Plant Sci*., 2017, **8**.

[32]. H. Yang, Y. Ren, X. Gao, and Y. Gao, *Chem. Res. Chin. Univ*., 2016, **32(6)**, 973-978.

[33]. P. Ghosh and A. Mandal, *Tetrahedron Lett*., 2012, **53**, 6483–6488.

[34]. S. Paul and B. Basu, *Tetrahedron Lett*., 2012, **53**, 4130–4133.

[35]. D. Zornik, R. M. Meudtner, T. E. Malah and C. M Thiele, *Hecht, S Chem. A Eur. J*., 2011, **17**, 1473–1484.

[36]. D. Yang, D. Fokas, J. Li, L. Yu and C. M. Baldino*, Synthesis*, 2005, **2005***,* 47–56.

[37]. H. J. Lim, D. Myung, I. Y. C. Lee, M. H. Jung, *J. Comb. Chem*., 2008, **10**, 501–503.

[38]. G. Csire, J. Demjén, S. Timári and K. Várnagy, *Polyhedron,* 2013, **61**, 202–212.

[39]. R. Kalarani, M. Sankarganesh, G. G. V. Kumar and M. Kalanithi, *J. Mol. Struct*., 2020, **1206**, 127725.

[40]. B. Bertrand, G. Gontard, C. Botuha and M. Salmain, *Eur. J. Inorg. Chem*., 2020, doi.org/10.1002/ejic.202000717.

[41]. C. K. Pal, S. Mahato, M. Joshi, S. Paul, A. R. Choudhury and B. Biswas, *Inorg. Chim. Acta*., 2020, **506**, 119541.

[42]. P. K. Mudi, N. Bandopadhyay, M. Joshi, M. Shit, S. Paul, A. R. Choudhury and B. Biswas, *Inorg. Chim. Acta*., 2020, **505**, 119468.

[43]. S. Mahato, N. Meheta, K. Muddukrishnaiah, M. Joshi, M. Shit, A. R. Choudhury and B. Biswas, *Polyhedron*, 2021, DOI. 10.1016/j.poly.2020.114933.

[44]. CrysAlisPro 1.171.39.35c, 2017, Rigaku Oxford Diffraction, Rigaku Corporation: Tokyo, Japan.

[45]. G. M. Sheldrick, *Acta Cryst*., 2015, **A71**, 3-8.

[46]. G. M. Sheldrick, *Acta Cryst*., 2015, **C71**, 3-8.

[47]. O. V. Dolomanov, L. J. Bourhis, R. J. Gildea, J. A. K. Howard and H. Puschmann, *J. Appl. Cryst*., 2009, **42**, 339-341.

[48]. M. J. Turner, J. J. McKinnon, S. K. Wolff, D. J. Grimwood, P. R. Spackman, D. Jayatilaka and M. A. Spackman, *Crystal Explorer* http://hirshfeldsurface.net17, 2017.

[49]. M. A. Spackman and D. Jayatilaka, *Cryst. Eng. Comm*., 2009, **11**, 19-32.

[50]. M. A. Spackman and J. J. McKinnon, *Cryst. Eng. Comm*., 2002, **4**, 378-392.

[51]. L. I. Simandi, S. Nemeth and N. Rumlis, *J. Mol. Catal*., 1987, **42**, 357.

[52]. M. Garai, D. Dey, H. R. Yadav, A. R. Choudhury, M. Maji and B. Biswas, *Chemistry Select*, 2017, **2**, 11040-11047.

[53]. S. Thakur, S. Banerjee, S. Das and S. Chattopadhyay, *New J. Chem*., 2019, **43**, 18747-18759.

[54]. R. K. Mahato, A. K. Mahanty, S. Paul, V. Gopal, B. Perumalsamy, G. Balakrishnan, T. Ramasamy, D. Dharumadurai and B. Biswas, *J. Mol. Struct*., 2021, **1223**, 129264.

[55]. B. Chowdhury, M. Maji and B. Biswas, *J. Chem. Sci*., 2017, **129**, 1627-1637.

[56]. C. K. Pal, S. Mahato, H. R. Yadav, M. Shit, A. R. Choudhury and B. Biswas, *Polyhedron*, 2019, **174**, 114156.

[57]. S. Ganguly, J. Mayans and A. Ghosh, *Chem Asian J*., 2020, **15**, 1–16.

[58]. S. Dutta, T. k. Ghosh, P. Mahapatra and A. Ghosh, *Inorg. Chem*., 2020, **59**,

14989−15003.

[59]. A. Mandal, S. Dasgupta, A. Adhikary, D. Samanta, E. Zangrando and D. Das, *Dalton Trans*., 2020, **49**, 5999.

[60]. S. Pal, B. Chowdhury, M. Patra, M. Maji and B. Biswas, *Spectrochim. Acta A. Mol. Biomol. Spectros*, 2015, **144**, 148–154.

[61]. S. Mahato and B. Biswas, *J. Indian Chem. Soc*., 2020, **97**, 849-856.

[62]. B. Chowdhury, B. Bhowmik, A. Sahu, M. Joshi, S. Paul, A.R. Choudhury and B. Biswas, *J. Chem. Sci*., 2018, **130**, 161.

[63]. A. K. Ghosh, A. Ali, Y. Singh, C. S. Purohit and R. Ghosh, *Inorg. Chim. Acta*., 2018, **474**, 156–163.

[64]. S. Sagar, S. Sengupta, A. J. Mota, S. K. Chattopadhyay, A. E. Ferao, E. Riviere, W. Lewis and S. Naskar, *Dalton Trans*., 2017, **46**, 1249–1259.

[65]. T. Dutta, S. Mirdya, P. Giri and S. Chattopadhyay, *Polyhedron*, 2020, **175**, 114164.